Talanta 250 (2022) 123683

Contents lists available at ScienceDirect

Talanta

journal homepage: www.elsevier.com/locate/talanta

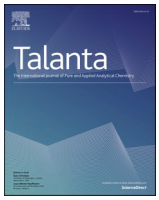

A highly-efficient 3D DNAzyme motor for sensitive biosensing analysis

Xia Zhong, Yunrui Li, Yuanyuan Chang, Ruo Yuan *, Yaqin Chai **

Key Laboratory of Luminescence Analysis and Molecular Sensing (Southwest University), Ministry of Education, College of Chemistry and Chemical Engineering, Southwest University, Chongqing, 400715, PR China

ARTICLE INFO

Keywords:
3D DNAzyme motor
DNAzyme nanowires
DNAzyme-amplified detection strategy
Electrochemical biosensing
DNA detection

ABSTRACT

Herein, driven by the need of highly-efficient DNAzyme-amplified detection strategy, a novel 3D DNAzyme motor was designed as a biosensor platform for realizing sensitive detection of target DNA. The 3D DNAzyme motor was composed of target-activated DNAzyme nanowires and substrates H1-Fc that co-immobilized on Au@Fe_3O_4 nanoparticles (Au@Fe_3O_4NPs) surface, possessing high local concentration of DNA reactants and shortened distance between DNAzyme and substrates for enhancing electrochemical signal. Compared with traditional DNAzyme-powered machines, the target-activated DNAzyme nanowires of 3D DNAzyme motor had greater flexibility and more powerful cleavage capability without troublesome sequence optimization, which overcame the space limitation and simultaneously interacted with adjacent and distant substrates H1-Fc to output a large amount of cleavage products with high signal response. Therefore, on account of the above-mentioned merits of nanoparticles localization DNA design and DNAzyme nanowires, the reported 3D DNAzyme motor ingeniously overcame many defects existing in traditional DNAzyme-amplified detection strategies such as low reactants concentration, limited flexibility of DNAzyme and small DNAzyme swing range, realizing the sensitive detection of target DNA with a detection limit of 1.7 fM ranging from 5 fM to 50 nM. Impressively, the 3D DNAzyme motor here presented a new strategy to achieve effective DNAzyme signal amplification and provided a reference for the assembly of various and functional 3D DNA machines in the future.

1. Introduction

DNA-based signal amplifying technology, including DNAzyme, hybridization chain reaction (HCR), catalyzed hairpin assembly (CHA), rolling circle amplification (RCA) [1–5], plays a powerful signal transduction function in biosensor platform and has been widely applied for sensitive analysis [6,7]. Among them, DNAzyme-amplified method is particularly attractive owing to the characteristics of low-cost, stability, cleavage specificity and adaptability [8–10]. Unfortunately, low DNAzyme cleavage efficiency still exists in these DNAzyme-amplified reaction, undoubtedly hampering their further applications in practical testing or other fields [11–13]. In fact, the reasons may be as follows: the recognition and interaction between DNAzyme and the corresponding substrates are easily affected by diffusion effect, but low concentration of reactants is commonly adopted in reactions for preventing unintended side reactions, which inevitably restricts the effective collision of reactants and brings negative effects.

Assembling DNAzyme nanowires is a common solution to improve DNAzyme cleavage efficiency [14–17]. In contrast to the traditional DNAzyme strands with only a DNAzyme functional domain, one DNAzyme nanowire contains multiple tandem DNAzyme functional domains and thereby directly increases the collision probability of DNAzyme towards substrates, which however only increases the local concentration of DNAzyme without considering local concentration of substrates. To be improved, researchers readily recruit DNAzyme and substrates simultaneously on nanoparticles surfaces to form the 3D DNAzyme machines with associate kinetics for accelerating the cleavage ability of DNAzyme [18]. Nevertheless, the freedom of DNAzyme is limited by a confined area, with poor mobility and small flexible swing range, resulting in the interaction with adjacent substrates only. Moreover, DNAzyme on nanoparticles surfaces always need to link with an optimized single-stranded spacer domain to ensure the outstanding flexibility and swing of strands, which is really a complex and time-consuming task [19–22]. Therefore, there are still some challenges to improve the DNAzyme-amplified detection strategies.

Based on the observation mentioned above, by integrating the advantages of DNAzyme nanowires and traditional 3D DNAzyme machines in the newly proposed DNAzyme amplification strategy, a highly

* Corresponding author.
** Corresponding author.

https://doi.org/10.1016/j.talanta.2022.123683
Received 7 December 2021; Received in revised form 6 June 2022; Accepted 10 June 2022
Available online 24 June 2022

efficient 3D DNAzyme motor was assembled and applied in a new biosensor for sensitively detecting target DNA that was related to oral cancer here. The relative design principle of 3D DNAzyme motor and the biosensor are illustrated in Scheme 1. First, the hairpin 1 labelled with ferrocene (H1-Fc) and the combination PST* probe assembled by primer, S1 and T* were prepared and then co-attached to Au@Fe_3O_4NPs surface. Once the target DNA was introduced, the target DNA recognized and captured the T* strands of PST* probe, leading the T* to release and triggering RCA to generate long DNAzyme strands with multiple repeating DNAzyme functional domains (DNAzyme nanowires). With the assistance of Mg^{2+}, these DNAzyme nanowires could recognize and rapidly cleave substrate H1-Fc. It is worth mentioning that the long length of DNAzyme nanowires fully improved the mobility and swing range of DNAzyme, making DNAzyme to overcome the space limitation and then simultaneously interact with adjacent and distant H1-Fc to output a large amount of cleavage products (S2-Fc) for further being captured on electrode to generate electrochemical signal. More importantly, the proposed 3D DNAzyme motor not only provides a new way to improve the DNAzyme-amplified detection strategy, but also further promotes the assembly of DNA machines with various functions and their development in biosensor platforms.

2. Experimental section

2.1. Preparation of AuNPs and Au@Fe_3O_4NPs

The synthesis of AuNPs referred to a previous method [23,24]. First, 2.0 mL $NaBH_4$ (1%) was quickly dispersed into 100 mL of boiling $HAuCl_4$ solution (0.01%) under stirring. After 15 min, the solution color turned to wine red, suggesting the successful formation of AuNPs. Next, the amino modified Fe_3O_4 nanoparticles (NH_2–Fe_3O_4NPs) were washed for three times by ultrapure water, which were mixed with the synthesized AuNPs for dealing with sonicate (15 min) and shaking (1 h) at 4 °C, leading to the linking of AuNPs onto the surface of NH_2–Fe_3O_4NPs by Au–N bonds. After magnetically separating for three times to disperse into the phosphate buffered saline (PBS), and then the Au@Fe_3O_4NPs were obtained.

2.2. Assembly and cleavage amplification of the 3D DNAzyme motor

In brief, equal molar quantities of DNA strands (primer, S1 and T*) were firstly mixed at a concentration of 2 μM, and then further heated to 95 °C for 5 min and slowly cooled to 4 °C to assemble PST* probe. Then, 5 μL PST* probe (2 μM), 100 μL annealed H1-Fc (2 μM) and 100 μL prepared Au@Fe_3O_4NPs were mixed and incubated for 12 h at room temperature. After magnetic separation and three times of washing, the obtained Au@Fe_3O_4-PST*-H1-Fc probe was stored in 100 μL PBS for the following experiments.

Subsequently, a mixture of Au@Fe_3O_4-PST*-H1-Fc (70 μL), T4 ligase (5 μL, 1 U/μL), Phi29 DNA polymerase (phi29, 5 μL, 2 U/μL) and deoxyribonucleotide triphosphates (dNTPs, 10 μL, 1 mM) was prepared. Once target DNA (10 μL) with various concentrations was added into the mixture, the T* strand of PST* probe could be captured by target DNA, thereby triggering RCA to generate long DNA strands with repeating DNAzyme units (DNAzyme nanowires) within 4 h [25,26], and further activating 3D DNAzyme motors. With the assistance of Mg^{2+}, DNAzyme nanowires of 3D DNAzyme motors thus began to recognize and cleave substrate H1-Fc. Importantly, with strong flexibility and large swing range, the DNAzyme nanowires here could interact with multiple H1-Fc at the same time to release numerous S2-Fc, which significantly enhanced the sensitivity of target analysis.

3. Results and discussion

3.1. Characterizations of AuNPs and Au@Fe_3O_4NPs

As displayed in Fig. 1A and B, the synthesized AuNPs seemed to be small particles in transmission electron microscopy (TEM) characterization, and were spherical and uniform in different sizes. In the subsequent Fig. 1C and D, we could see that many AuNPs attached to the uniform Fe_3O_4NPs surface with a diameter of about 100 nm.

Besides, x-ray photoelectron spectrometer (XPS) was employed for elemental analysis to further confirm Au@Fe_3O_4NPs. As can be seen from Fig. 2, the typical peaks of Au 4f, Fe 2p, O 1s and C 1s were clearly observed in the synthetic Au@Fe_3O_4NPs spectrum, reflecting that the Au, Fe, O and C were presented in the prepared sample, respectively. These results all proved that the Au@Fe_3O_4NPs here were synthesized

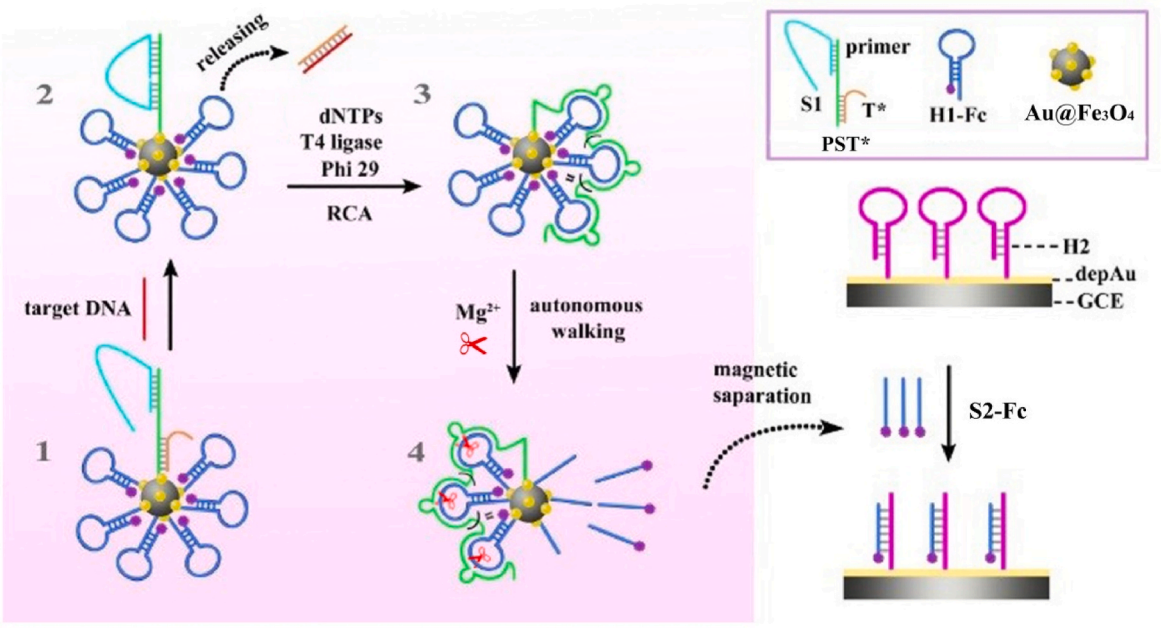

Scheme 1. Schematic diagram of the proposed biosensor for target DNA analysis based on 3D DNAzyme motor.

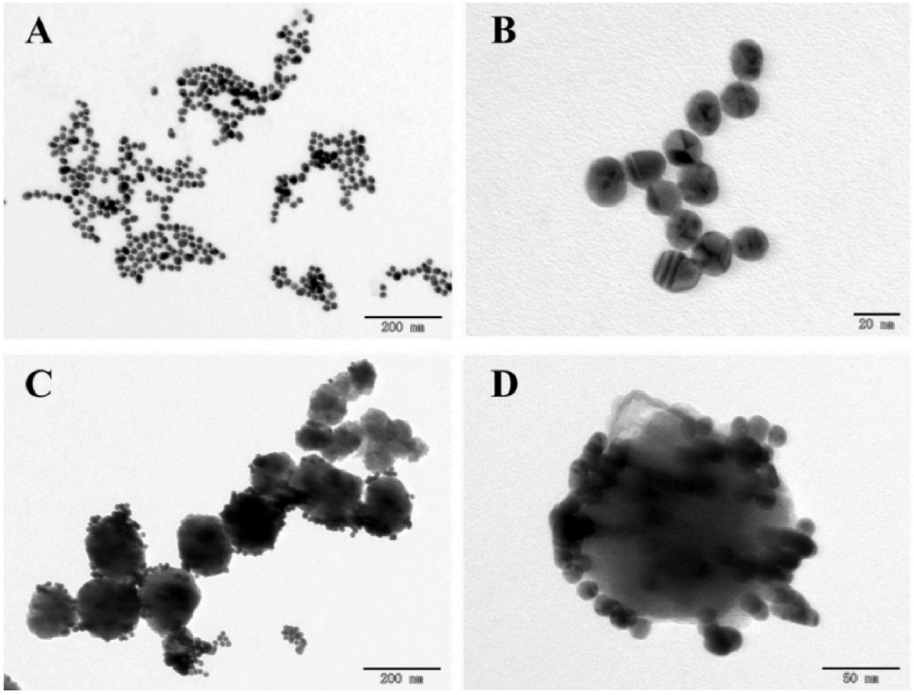

Fig. 1. TEM characterizations of AuNPs within different scales: (A) 200 nm and (B) 20 nm, TEM characterization of Au@Fe_3O_4NPs within different scales: (C) 200 nm and (D) 50 nm.

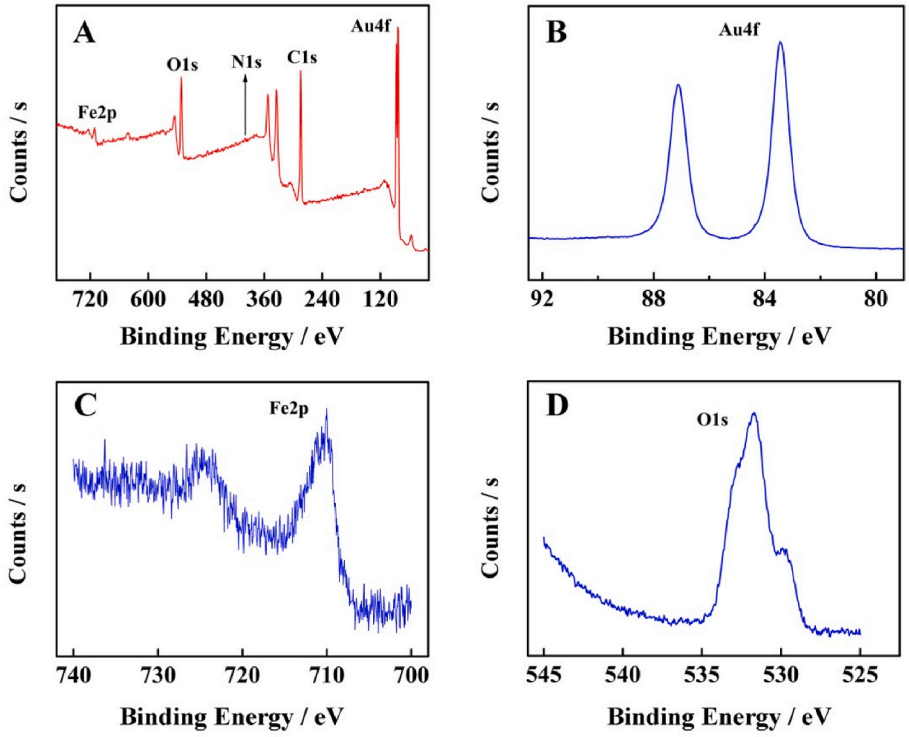

Fig. 2. XPS spectra for the full region of (A) Au@Fe_3O_4, (B) Au 4f region, (C) Fe 2p region, and (D) O 1s region.

successfully.

3.2. Polyacrylamide gel electrophoresis (PAGE)

PAGE is an indispensable method to demonstrate the successful assembly of DNA structures. As illustrated in Fig. 3A, all prepared samples were analyzed by 16% nondenaturing polyacrylamide gels at 120 V. Lane 1, lane 2, lane 3, and lane 4 corresponded to target DNA, primer, S1 and T*, respectively. After annealing the mixture of primer, S1 and T*, a bright band with slow migration appeared in lane 5, indicating the successful preparation of PST* probe. And the lane 6 matched with the hybridization result of PST* probe and target DNA. In detail, the target DNA captured the T* strand in the PST* probe, outputting products of primer-S1 and Target DNA-T*, thereby corresponding to the two new

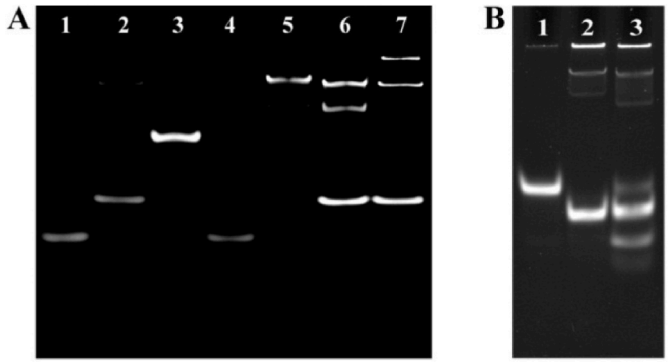

Fig. 3. PAGE results for different samples. (A): target DNA (lane 1), primer (lane 2), S1 (lane 3), T* (lane 4), the annealing result of primer, S1 and T* (lane 5), the hybridization result of target DNA and PST* (lane 6), the rolling circle amplification products (lane 7). (B): H1 (lane 1), the rolling circle amplification products (lane 2), the reaction result between H1 and rolling circle amplification products (lane 3).

bands in the lane. Subsequently, with the addition of T4 ligase, phi 29 and dNTPs, low mobility products were obtained in lane 7, in which the highest band demonstrated the assembling of DNAzyme nanowires. These results confirmed that the PST* probe synthesis was successful and the target DNA could trigger RCA process.

To further characterize the cleavage capacity of DNAzyme nanowires obtained by RCA, a PAGE experiment was also performed. As can be seen from Fig. 3B, the lane1 and lane 2 represented H1 and RCA products including DNAzyme nanowires, respectively, once H1 was mixed and incubated with the DNAzyme nanowires, two lower bands appeared in lane 3, which strongly proved that the DNAzyme nanowires were indeed able to recognize and cleavage H1 as we expected.

3.3. Stepwise characterization of the modified electrode

The modified electrode was monitored by cyclic voltammetry (CV) and electrochemical impedance spectroscopy (EIS), respectively. As shown in Fig. 4A, the characteristic peaks of $[Fe(CN)_6]^{3-/4-}$ were obtained from the bare glassy carbon electrode (GCE) (curve a). While deposited Au (depAu) was immobilized on the bare GCE (depAu/GCE), the electrochemical signal increased (curve b) because of the preeminent conductivity of depAu. When depAu/GCE was incubated with H2, a decreasing electrochemical signal was obtained (curve c) due to the negative charge of H2 (H2/depAu/GCE). Fig. 4B was the corresponding EIS curves of the modified electrode. The value of electron-transfer resistance (R_{et}) of depAu/GCE significantly decreased (curve b) when compared with bare GCE (curve a), proving the excellent conductivity of depAu. And with the introduction of H2 to depAu/GCE, an increasing R_{et} response was observed (curve c). These obtained results stayed the same with the CV characterizations, demonstrating the successful construction of the proposed electrode once again.

3.4. Feasibility of the electrochemical biosensor

To prove the feasibility of electrochemical biosensor, the square wave voltammetry (SWV) measurement was performed in PBS solution to monitor different modified electrodes. As displayed in Fig. 5, when the H2/depAu/GCE was measured, a smooth curve (curve a) was recorded. Once the H2/depAu/GCE was further treated with the cleavage products of 3D DNAzyme motor, the typical oxidation peak of Fc presented (about 0.45 V), which obviously demonstrated that S2-Fc was able to be captured on the electrode surface successfully. These results well proved that the as-prepared biosensor could offer a new strategy to perform target analysis.

3.5. Optimization of the reaction conditions

In this work, the sensitivity of sensor is closely related to the cleavage reaction of 3D DNAzyme motor, and the cleavage reaction involves both PST* probe and H1-Fc, thus, the concentration ratio of PST* probe to H1-Fc were optimized. SWV was used to explore the response of biosensor with sever ratios (from 1:1 to 1:30). As showed in Fig. 6A, the electrochemical signal increased to the maximum at 1:20 when the ratio increasing from 1:1 to 1:30. Thus, the optimal ratio for subsequent experiments was chosen at 1:20. Further, the cleavage reaction of

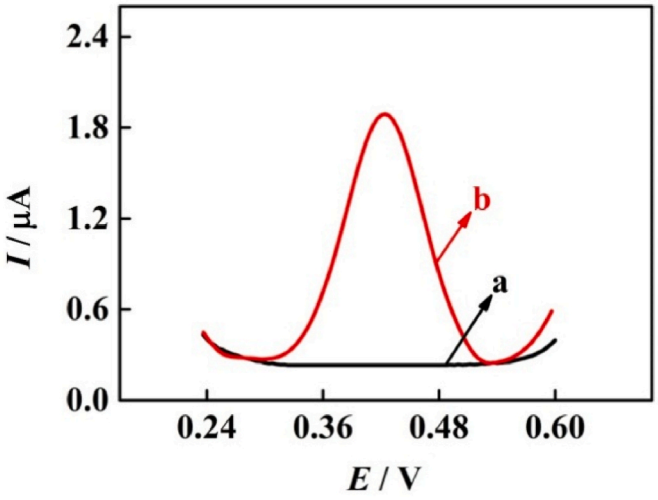

Fig. 5. SWV responses of (a) H2/depAu/GCE and (b) H2/depAu/GCE after treating with the cleavage products of 3D DNAzyme motor (0.1 nmol/L target DNA).

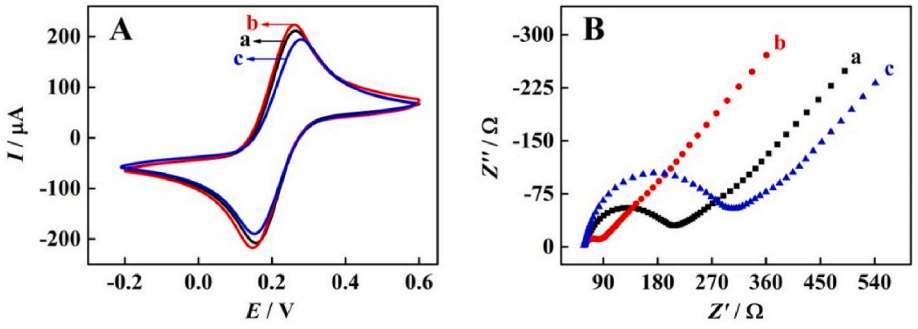

Fig. 4. (A) CV and (B) EIS characterizations of modified electrode at different stages in 5 mM $[Fe(CN)_6]^{3-/4-}$ solution: (a) bare GCE, (b) depAu/GCE, (c) H2/depAu/GCE.

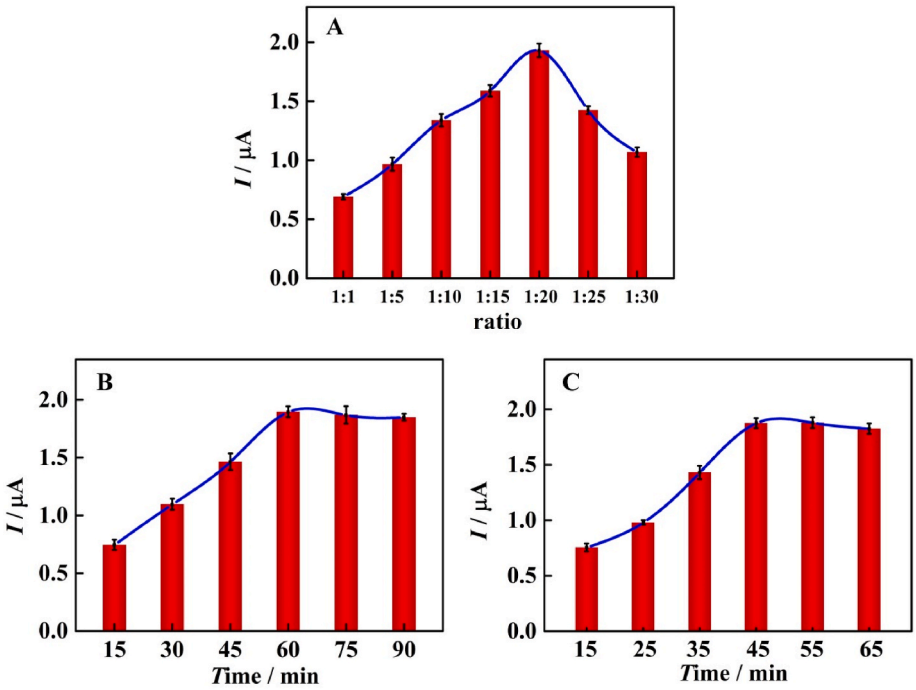

Fig. 6. (A) Influence of the concentration ratios between PST* and H1-Fc toward SWV response (1:1, 1:5, 1:10, 1:15, 1:20, 1:25, 1:30). (B) Effect of cleavage time of 3D DNAzyme motor on electrode response. (C) Optimum incubation time of S2-Fc. The current values were obtained with 10 pM target DNA in PBS solution. Error bars: SD, $n = 3$.

DNAzyme nanowires of 3D DNAzyme motor toward H1-Fc was significantly step to improve the biosensor performance, therefore the cleavage time (15 min, 30 min, 45 min, 60 min, 75 min, 90 min) of 3D DNAzyme motor on electrode was also studied. As can be seen from that the electrochemical signal greatly rose with the increasing cleavage time till 60 min, proving the adequate cleavage reaction could be selected as 60 min (Fig. 6B). Furthermore, the immobilization time of cleavage products of 3D DNAzyme motor (S2-Fc) on H2/depAu/GCE would affect the capture of H2, further leading to influence the biosensor performance. Thus, we also estimated the immobilization time of S2-Fc. As can be seen from Fig. 6C, the current value rose with the increasing time and arrived at its maximum at 45 min. Thus, 45 min was regarded as the optimum immobilization time of S2-Fc and used in the subsequent experiments.

3.6. Electrochemical assay of target DNA

Target DNA with different concentrations was measured to estimate the analysis ability of the proposed electrochemical biosensor under optimal experimental conditions. As shown in Fig. 7A, the electrochemical response of peak current increased with the increase of target DNA concentration. Concurrently, by adopting the logarithm of target DNA concentration as abscissa and the I_{Fc} as ordinate, the calibration curve was also established, proving a good linear relationship between I_{Fc} and the logarithm of target DNA concentration ranging from 5 fM to 50 nM (Fig. 7B). And the corresponding linear regression equation was $I = 0.3712 \lg c + 2.621$ ($r = 0.9965$) with the detection limit of 1.7 fM (S/N = 3), demonstrating that the proposed 3D DNAzyme motor here showed excellent DNAzyme cleavage capacity. Thus, the 3D DNAzyme molecular motor had the potential to be used as a novel and powerful DNAzyme amplification detection tool in the detection of other nucleic acids.

3.7. Selectivity, reproducibility and stability of the biosensor

For investigating the selectivity of biosensor, interference tests were conducted to analyze various interfering species (miR-21, miR-141, miR-155, HIV, AD-DNA, and the mixture). As illustrated in Fig. 8A, when these interferences were respectively tested, the current values were almost negligible despite the concentrations of interferences as

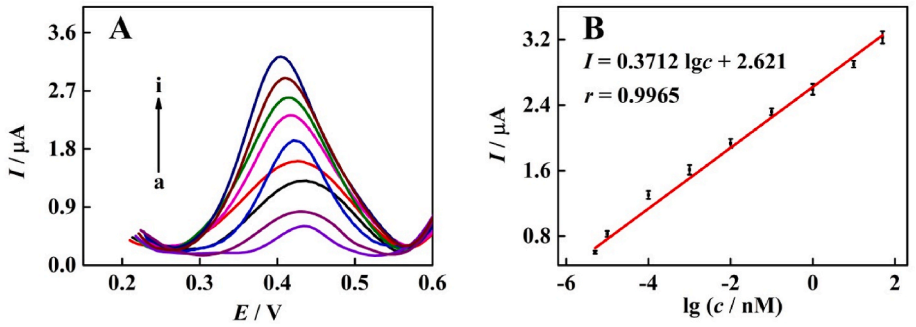

Fig. 7. (A) SWV responses of proposed biosensor incubated with various target DNA concentrations (from a to i): 5 fM, 10 fM, 100 fM, 1 pM, 10 pM, 100 pM, 1 nM, 10 nM and 50 nM in PBS. (B) Calibration plot of peak current *vs* the logarithm of target DNA concentration. Error bars: SD, $n = 3$.

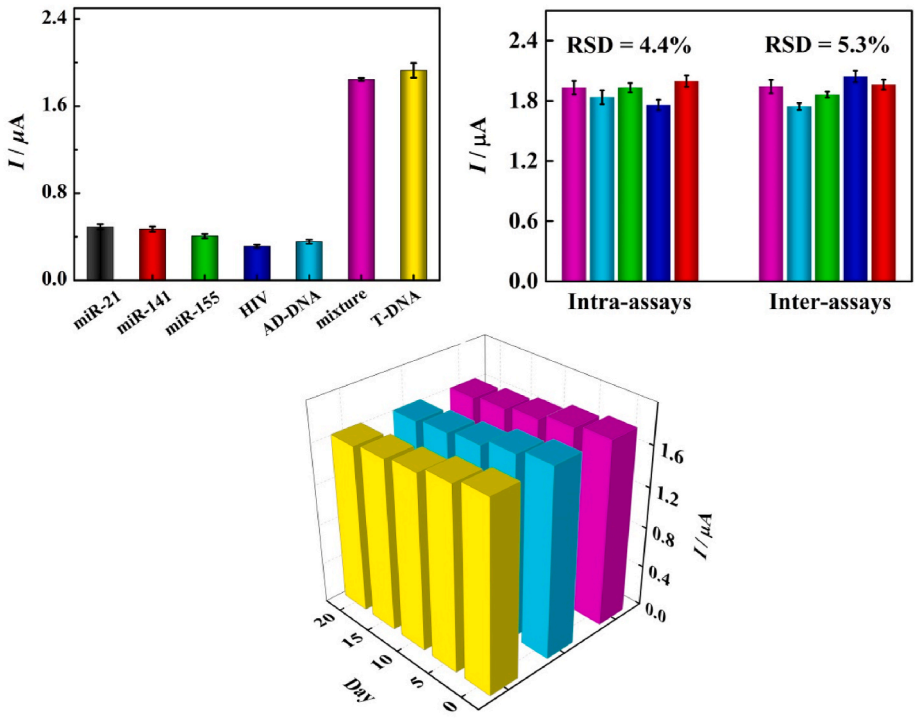

Fig. 8. (A) Selectivity of proposed biosensor for target DNA (10 pM) against other interferes (each at 1 nM), (B) The intra- and inter-assays of biosensor (10 pM target DNA), (C) Stability of the proposed biosensor (10 pM target DNA). Error bars: SD, $n = 3$.

high as 1 nM. When the mixture of all interferes and target DNA was tested, the I_{Fc} value with a sharp increase was obtained as same as the only presence of target DNA. It can be concluded that once a small amount of target DNA (10 pM) were measured, the I_{Fc} values rapidly raised and higher than that of interference tremendously, proving that the fabricated biosensor presented high selectivity for target DNA against other interferes. Next, we prepared five biosensors in the same batch and five different batches of biosensors, for studying the intra-batch and inter-batch reproducibility. As shown in Fig. 8B, the response signals of these different biosensors were roughly same and the relative standard deviation (RSD) were 4.4% and 5.3% respectively, proving a good reproducibility of the biosensor.

Moreover, by storing the as-prepared biosensor at 4 °C and measuring intermittently (every 5 days), the stability of biosensor was analyzed. After 20 days, the electrochemical signal of the biosensor was still kept at 89.3% of its initial value, demonstrating that the as-prepared biosensor possessed good stability (Fig. 8C).

4. Conclusion

In general, a novel 3D DNAzyme motor was designed in this work and applied to electrochemical sensing platform for sensitive target DNA detection. The assembly of DNAzyme molecular motors here combined the merits of DNAzyme nanowires and traditional DNAzyme machines, considering that these two methods could draw on each other's strengths to offset weaknesses and complement each other, which showed many laudable features as follows: First, both DNAzyme nanowires and substrates (H1-Fc) had high local effective concentration, enhancing detection sensitivity. Second, due to their length and flexibility, the DNAzyme nanowires in the motor could recognize and cleave adjacent and distant H1-Fc at the same time without being constrained by space, thus solving many problems existing in the traditional DNAzyme motor including limited mobility of DNAzyme, small swing range, and troublesome sequence optimization. Third, the 3D DNAzyme motor of not only realized the DNAzyme-amplified target detection and promoted the development of DNA nanomachines in the biosensor platform, but also provided a reference for the future assembly of DNA machines with various functions.

Author contributions

Xia Zhong: Conceptualization, Formal analysis, Data curation, Writing - original draft. **Yunrui Li:** Conceptualization, Investigation. **Yuanyuan Chang:** Conceptualization, Investigation. **Yaqin Chai:** Conceptualization, Writing - review & editing, Supervision, Project administration, Funding acquisition. **Ruo Yuan:** Conceptualization, Writing - review & editing, Supervision, Project administration, Funding acquisition.

Declaration of competing interest

The authors declare that they have no known competing financial interests or personal relationships that could have appeared to influence the work reported in this paper.

Acknowledgements

This paper was financially supported by the National Natural Science Foundation of China (21904108, 21775124) and the Fundamental Research Funds for the Central Universities (XDJK2018AA003), China.

Appendix A. Supplementary data

Supplementary data to this article can be found online at https://doi.org/10.1016/j.talanta.2022.123683.

References

[1] K.W. Ren, Y.F. Xu, Y. Liu, M. Yang, H.X. Ju, A responsive "nano string light" for highly efficient mRNA imaging in living cells via accelerated DNA cascade reaction, ACS Nano 12 (2018) 263–271.
[2] J. Zhang, M.Y. He, C.P. Nie, M.M. He, Q.S. Pan, C. Liu, Y.L. Hu, J.T. Yi, T.T. Chen, X. Chu, Biomineralized metal-organic framework nanoparticles enable enzymatic

rolling circle amplification in living cells for ultrasensitive MicroRNA imaging, Anal. Chem. 91 (2019) 9049–9057.
[3] P. Qin, L. Yao, J. Xu, G. Liu, W. Chen, Smart engineering of a dual-DNA machine with a high signal-to-noise ratio for one-pot robust and sensitive miRNA signaling, Chem. Commun. 55 (2019) 14367–14370.
[4] H.Y. Peng, A.M. Newbigging, Z.X. Wang, J. Tao, W.C. Deng, X.C. Le, H.Q. Zhang, DNAzyme-mediated assays for amplified detection of nucleic acids and proteins, Anal. Chem. 90 (2018) 190–207.
[5] F.C. Simmel, B. Yurke, H.R. Singh, Principles and applications of nucleic acid strand displacement reactions, Chem. Rev. 119 (2019) 6326–6369.
[6] M. Trotter, N. Borst, R. Thewes, F. Stetten, Electrochemical DNA Sensing-Principles, commercial systems, and applications, Biosens. Bioelectron. 154 (2020), 112069.
[7] L.L. Zhang, R. Abdullah, X.X. Hu, H.R. Bai, H.H. Fan, L. He, H. Liang, J.M. Zou, Y. L. Liu, Y. Sun, X.B. Zhang, W.H. Tan, Engineering of bioinspired, size-controllable, self-degradable cancer-targeting DNA nanoflowers via the incorporation of an artificial sandwich base, J. Am. Chem. Soc. 141 (2019) 4282–4290.
[8] H.H. Liu, X. Yu, Y.Q. Chen, J. Zhang, B.X. Wu, L. Zheng, P. Haruehanroengra, R. Wang, S.H. Li, J.Z. Lin, J.X. Li, J. Sheng, Z. Huang, J.B. Ma, J.H. Gan, Crystal structure of an RNA-cleaving DNAzyme, Nat. Commun. 8 (2017) 1–10.
[9] J. Wang, H.M. Wang, H. Wang, S.Z. He, R.M. Li, Z. Deng, X.Q. Liu, F. Wang, Nonviolent self-catabolic DNAzyme nanosponges for smart anticancer drug delivery, ACS Nano 13 (2019) 5852–5863.
[10] T.H. Peng, Z.Y. Deng, J.X. He, Y.Y. Li, Y. Tan, Y.B. Peng, X.Q. Wang, W.H. Tan, Functional nucleic acids for cancer theranostics, Coord. Chem. Rev. 403 (2020), 213080.
[11] F. Wang, J. Elbaz, R. Orbach, N. Magen, I. Willner, Amplified analysis of DNA by the autonomous assembly of polymers consisting of DNAzyme wires, J. Am. Chem. Soc. 133 (2011) 17149–17151.
[12] H. Chai, P. Miao, Bipedal DNA walker based electrochemical genosensing strategy, Anal. Chem. 91 (2019) 4953–4957.
[13] S. Lilienthal, M. Klein, R. Orbach, I. Willner, F. Remacle, R.D. Levine, Continuous variables logic via coupled automata using a DNAzyme cascade with feedback, Chem. Sci. 8 (2017) 2161–2168.
[14] H. Wang, H.M. Wang, Q. Wu, M.J. Liang, X.Q. Liu, F. Wang, A DNAzyme-amplified DNA circuit for highly accurate microRNA detection and intracellular imaging, Chem. Sci. 10 (2019) 9597–9604.
[15] D.G. He, X. He, X. Yang, H.W. Li, A smart ZnO@polydopamine-nucleic acid nanosystem for ultrasensitive live cell mRNA imaging by the target-triggered intracellular selfassembly of active DNAzyme nanostructures, Chem. Sci. 8 (2017) 2832–2840.
[16] M. Liu, Q. Zhang, D. Chang, J. Gu, J.D. Brennan, Y.F. Li, A DNAzyme feedback amplification strategy for biosensing, Angew. Chem. 129 (2017) 1–6.
[17] L.L. Zhang, J.J. Zhao, J.H. Jiang, R.Q. Yu, Target-activated autocatalytic DNAzyme amplification strategy for the assay of base excision repair enzyme activity, Chem. Commun. 48 (2012) 8820–8822.
[18] M. Qing, S.B. Xie, W. Cai, D.Y. Tang, Y. Tang, J. Zhang, R. Yuan, Click chemistry reaction-triggered 3D DNA walking machine for sensitive electrochemical detection of copper ion, Anal. Chem. 90 (2018) 11439–11445.
[19] J. Wang, D.X. Wang, A.N. Tang, D.M. Kong, Highly integrated, biostable, and self-powered DNA motor enabling autonomous operation in living bodies, Anal. Chem. 91 (2019) 5244–5251.
[20] J.B. Chen, A. Zuehlke, B. Deng, H.Y. Peng, X.D. Hou, H.Q. Zhang, A target-triggered DNAzyme motor enabling homogeneous, amplified detection of proteins, Anal. Chem. 89 (2017) 12888–12895.
[21] H.Y. Peng, X.F. Li, H.Q. Zhang, X.C. Le, A microRNA-initiated DNAzyme motor operating in living cells, Nat. Commun. 8 (2017), 14378.
[22] N.M. Hu, Y.F. Wang, C. Liu, M.M. He, C.P. Nie, J. Zhang, Q.Q. Yu, C. Zhao, T. T. Chen, X. Chu, An enzyme-initiated DNAzyme motor for RNase H activity imaging in living cell, Chem. Commun. 56 (2020) 639–642.
[23] Z.Q. Xu, L.L. Liao, Y.Q. Chai, H.J. Wang, R. Yuan, Ultrasensitive electrochemiluminescence biosensor for MicroRNA detection by 3D DNA walking machine based target conversion and distance-controllable signal quenching and enhancing, Anal. Chem. 89 (2017) 8282–8287.
[24] Y. Shan, J.J. Xu, H.Y. Chen, Opto-magnetic interaction between electrochemiluminescent CdS : Mn film and Fe_3O_4 nanoparticles and its application to immunosensing, Chem. Commun. 46 (2010) 4187–4189.
[25] C. Yao, H.D. Qi, X.M. Jia, Y.W. Xu, Z.B. Tong, Z. Gu, D.Y. Yang, A DNA nanocomplex containing cascade DNAzymes and promoter-like Zn-Mn-ferrite for combined gene/chemo-dynamic therapy, Angew. Chem. Int. Ed. 61 (2022), e202113619.
[26] J. Wang, S.S. Yu, Q. Wu, X. Gong, S.Z. He, J.H. Shang, X.Q. Liu, F.A. Wang, A self-catabolic multifunctional DNAzyme nanosponge for programmable drug delivery and efficient gene silencing, Angew. Chem. 133 (2021) 10861–10869.